*Journal of Sound and Vibration* (2002) **249**(4), 679–700
doi:10.1006/jsvi.2001.3817, available online at http://www.idealibrary.com on IDEAL®

# NOISE GENERATED BY A COANDA WALL JET CIRCULATION CONTROL DEVICE

M. S. Howe

*Boston University, College of Engineering, 110 Cummington Street, Boston MA 02215, U.S.A.*

(*Received* 13 *November* 2000, *and in final form* 10 *May* 2001)

An analysis is made of the production of sound by a hydrofoil with a Coanda wall jet circulation control (CC-) device. Three principal sources are identified in the vicinity of the trailing edge of the hydrofoil. The radiation at very low frequencies is dominated by "curvature noise" generated by the interaction of boundary layer turbulence with the rounded trailing edge of the CC-hydrofoil; this is similar in character and magnitude to the low-frequency component of the conventional trailing edge noise produced by a hydrofoil of the same chord, but with a sharp trailing edge. Higher frequency sound is produced principally at the Coanda jet slot. "Passive slot noise" is caused by the "scattering" by the slot lip of nearfield pressure fluctuations in the turbulent boundary layer of the exterior mean flow past the slot. This is of comparable intensity to high frequency, sharp-edged trailing edge noise. However, the acoustic spectrum is greatly extended to much higher frequencies if the Coanda jet is turbulent; the sound produced by the interaction of this turbulence with the lip tends to dominate the spectrum at frequencies $f$ (Hz) greater than about $U_j/h$, where $h$ is the slot width and $U_j$ the Coanda jet speed. Sample numerical results are presented for a typical underwater application that indicate that at this and higher frequencies the slot noise can be 20 dB or more greater than conventional trailing edge noise, although the differences become smaller as the thickness of the slot lip increases.



## 1. INTRODUCTION

A jet directed tangentially over a rounded solid surface tends to cling to the surface in a manner familiarly attributed to the *Coanda effect*. The phenomenon was studied by Coanda [1] in the 1930s, but had been noted as early as 1800 [2, 3]. The curved trajectory of a fluid particle in the jet close to the surface is governed by a balance at high Reynolds numbers between its centrifugal inertia force and the "radial" pressure gradient, and many such flows are well described analytically by methods of potential flow theory [4, 5]. However, viscous frictional forces at the surface are necessary to produce the initial deflection of the jet towards the curved wall.

A Coanda *circulation control* (CC) device consisting of a high-speed two-dimensional jet discharging from a slot towards the trailing edge of an airfoil on the suction side has been extensively investigated because it can greatly increase the airfoil lift coefficient [5–12]. When the trailing edge is suitably rounded the jet follows the curved surface causing the mean air flow over the airfoil to remain attached and delaying separation until the flow reaches a point on the "pressure" side of the airfoil effectively corresponding to that predicted for potential flow with the same total circulation. The airfoil can thereby attain a maximum lift that is many times larger than that of a conventional airfoil. In particular,

0022-460X/02/040679 + 22 $35.00/0 

circulation control enables high lift to be achieved at low flight speeds and at small or zero angles of attack; also, it can replace mechanical lift augmentation systems, such as trailing edge flaps. A Coanda jet can deflect downwards, around the rounded trailing edge of a wing, the mean jet flow from a turbofan engine mounted above the wing (configured for "upper surface blowing") [5]. This permits the direction of thrust to be controlled by adjusting the Coanda jet speed, a procedure that allows almost instantaneous "thrust vectoring" and the attainment of the very high lifts required for vertical flight without the need to deploy mechanical high lift devices. Pulsing the Coanda jet has also been proposed as a means of controlling airfoil vibration [13].

But the introduction of circulation control can involve large increases in the noise generated by turbulence interacting with the airfoil. Thus, upper surface blowing greatly increases turbofan jet noise (by 25 dB or more), caused by the "diffraction" of jet shear layer pressures by the wing trailing edge; *additional* increases of as much as 30 dB are observed at high frequencies when CC is applied to deflect the jet for thrust vectoring, presumably produced by the interaction of turbulence in the (near sonic) Coanda jet with the jet slot [14]. Carpenter *et al.* [2, 15] stressed the importance of the jet slot as a source of sound at supersonic Coanda jet speeds, for both smoothly contoured and "stepped" slots. For the contoured slot the dependence of the overall sound power on jet speed $U$ was approximately proportional to $U^8$, in accordance with Lighthill's theory of the generation of aerodynamic sound by "freefield" turbulence quadrupoles [16]; for a slot with a step no clear velocity dependence was evident, but the sound power at low speeds varied much more slowly with $U$, indicating the increased importance of surface interaction noise sources at these speeds [17].

This suggests that turbulence–slot interaction noise is probably the most important component of the sound generated by a Coanda CC device at low speeds. In underwater applications circulation control of a *hydrofoil* is a potentially attractive means of augmenting lift at very low speeds and small angles of attack. The analytical problem of predicting the accompanying acoustic radiation, especially at higher frequencies, is the subject of this paper. At very small Mach numbers the direct radiation of sound from turbulence quadrupoles is usually of no practical importance. Our analysis identifies four distinct surface-source self-noise mechanisms: (1) the interaction of the turbulent shear layers in the Coanda jet with the jet slot; the interaction of exterior boundary layer turbulence with (2) the jet slot and (3) the rounded trailing edge; and (4) a weak surface interaction of boundary layer turbulence at the separation point on the pressure side of the hydrofoil. Mechanisms (2) and (3) are found to be important at low frequencies at mean ambient flow speeds of a few meters per second; higher frequencies are dominated by the Coanda jet source (1); separation noise (4) is confined to very low frequencies and amplitudes.

These conclusions are based on an analysis of the production of sound by a two-dimensional hydrofoil with a rounded trailing edge fitted with a Coanda CC device close to the edge. The noise problem is formulated in section 2 of this paper, and a qualitative estimate is made of the relative importance of mechanisms (3) and (4). Prediction formulae for noise mechanisms (1), (2) and (3) are derived in sections 3 and 4. A sample application of these formulae is made in section 5. This includes a comparison with the conventional "trailing edge noise" produced by a nominally identical mean flow past the trailing edge of a thin hydrofoil of the same chord, but with no circulation control [17]. Of course, the Coanda jet of a "well designed" CC-device should be laminar. In that case, the jet would make no direct contribution to the interaction noise, although entrainment by the jet is still likely to modify the amplitude of the sound generated by the exterior boundary layer turbulence.

## 2. EQUATIONS FOR THE HYDROACOUSTIC RADIATION

### 2.1. INTEGRAL REPRESENTATIONS

Consider a two-dimensional CC-hydrofoil set at zero angle attack in a uniform, high Reynolds number mean flow at speed $U$ in the positive $x_1$ direction of the rectangular co-ordinate system $(x_1, x_2, x_3)$ (see Figure 1, where the $x_3$-axis is taken in the spanwise direction, out of the plane of the paper). To fix ideas the profile S of the hydrofoil may be assumed to be nominally of elliptic cross-section, except downstream of the spanwise Coanda jet slot, where the profile becomes a circular arc of radius $\mathfrak{R}$. The mean fluid density and sound speed are denoted, respectively, by $\rho_0$ and $c_0$, and the mean flow Mach number $M = U/c_0$ may be regarded as infinitesimal. Sound is generated by the turbulence within the boundary layers on S and also in the jet flow from the slot. At the very low Mach numbers of underwater applications the principal mechanism of sound production is the diffraction of the nearfield turbulence pressures by variations in surface geometry; the direct radiation from turbulence quadrupole sources (whose intensity varies as $\rho_0 U^3 M^5$) can be ignored.

In these circumstances the acoustic pressure $p(\mathbf{x}, t)$ at position $\mathbf{x}$ and time $t$ can be represented in the form

$$p(\mathbf{x}, t) = -\rho_o \int \frac{\partial G}{\partial \mathbf{y}}(\mathbf{x}, \mathbf{y}, t-\tau) \cdot (\boldsymbol{\Omega} \wedge \mathbf{v})(\mathbf{y}, \tau)\, \mathrm{d}^3\mathbf{y}\, \mathrm{d}\tau, \quad |\mathbf{x}| \to \infty, \tag{1}$$

where $\mathbf{v}$ and $\boldsymbol{\Omega} = \operatorname{curl} \mathbf{v}$ are, respectively, the fluid velocity and vorticity. This formula is applicable for low Mach number, high Reynolds number flows, when the contribution to sound production by surface skin friction sources is of no significance [17]. $G(\mathbf{x}, \mathbf{y}, t-\tau)$ is an acoustic Green function, which satisfies

$$(\partial^2/c_0^2 \partial t^2 - \nabla^2) G = \delta(\mathbf{x}-\mathbf{y})\delta(t-\tau), \quad G(\mathbf{x}, \mathbf{y}, t-\tau) = 0 \quad \text{for } t < \tau, \tag{2}$$

such that $\partial G(\mathbf{x}, \mathbf{y}; t-\tau)/\partial y_n = 0$, $\partial G(\mathbf{x}, \mathbf{y}; t-\tau)/\partial x_n = 0$, respectively, for $\mathbf{y}$ and $\mathbf{x}$ on S, where $y_n$ and $x_n$ are measured from S in the direction of the unit normal $\mathbf{n}$ (directed into the fluid).

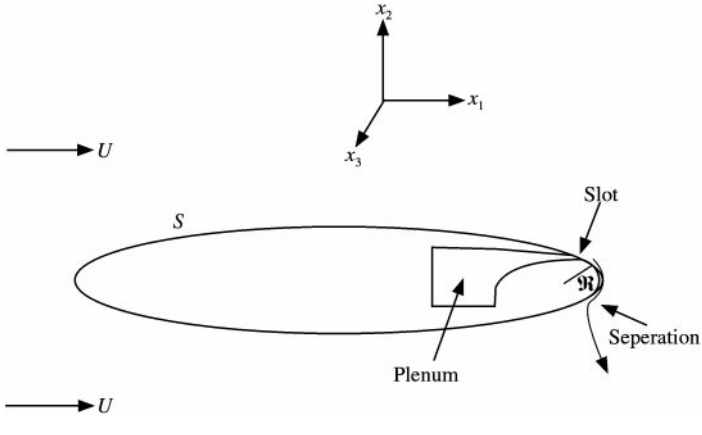


Figure 1. Schematic Coanda jet circulation control hydrofoil, set at zero angle of attack to a nominally uniform mean flow at speed $U$, showing the jet slot and plenum.

Equation (1) is a useful representation of the sound only when the unsteady velocity and vorticity are known, and is applied below in section 2.2. For predictive purpose, however, it is more convenient to adopt an indirect measure of the turbulent field obtained from observations or modelling of the *unsteady surface pressures*. This can be done by using the following alternative, but equivalent, low Mach number representation [18]:

$$p(\mathbf{x}, t) = -\rho_0 \oint_S G(\mathbf{x}, \mathbf{y}, \mathbf{t} - \tau) \frac{\partial v_n}{\partial \tau}(\mathbf{y}, \tau)\, \mathrm{d}S(\mathbf{y})\, \mathrm{d}\tau, \tag{3}$$

where $G(\mathbf{x}, \mathbf{y}, t - \tau)$ is defined as in equation (1), and $v_n$ is the normal component (directed into the fluid) of the *upwash* velocity $v$ of the turbulence for *incompressible* flow, which is formally defined in terms of the vorticity by the Biot–Savart formula [19]

$$\mathbf{v}(\mathbf{x}, t) = \mathrm{curl} \int_{V_\delta} \frac{\boldsymbol{\Omega}(\mathbf{y}, t)\, \mathrm{d}^3\mathbf{y}}{4\pi|\mathbf{x} - \mathbf{y}|}, \tag{4}$$

the integration being confined to the non-linear region $V_\delta$ of the flow *outside* the viscous sublayers on S (i.e., excluding "bound" vorticity on S) [18]. Representation (3) is equivalent to the "diffraction theory" method of calculating the aerodynamic sound that was introduced by Chase [20, 21] and by Chandiramani [22] to study trailing edge noise, and is a natural development of Sears' [23] treatment of the "gust loading" problem for a thin airfoil.

Applications of equation (3) strictly depend on a knowledge of the vorticity $\boldsymbol{\Omega}$. However, the upwash velocity can also be well approximated from measurements or by using a suitable empirical model of the surface pressure fluctuations on S. Observe that $\mathbf{v}(\mathbf{x}, t)$ is the "kinematic" velocity induced by the vortex field $\boldsymbol{\Omega}$ when the influence of "image" vortices within S is ignored.

### 2.2. SOURCE IDENTIFICATION

The base level radiation from the hydrofoil is the sound produced when the contribution from any turbulence in the Coanda circulation control jet is ignored. If turbulence levels in the incident mean flow are negligible the primary sources are then associated with the growth of the turbulent boundary layers on S. The sound from this source can be estimated independently of the contribution from the Coanda jet, and consists of sound generated when the turbulence is swept past the surface irregularity formed by the slot, by its interaction with the "trailing edge" of the hydrofoil (which in this case means the region of maximum surface "sharpness" or curvature), and also by the surface reaction force produced by the rapid acceleration of turbulence away from the hydrofoil in the vicinity of the separation zone. Of these mechanisms the slot interaction source will occupy the higher frequency portion of the acoustic spectrum, and is considered in detail in section 4. The curvature and separation sources are significant only at low frequencies $\sim U/\mathfrak{R}$.

The relative importance of these two low-frequency sources can be estimated by considering their contributions to the sound generated by a spanwise line vortex, imagined to be inserted into the boundary layer on the suction side of the hydrofoil far upstream of the slot and then to be convected (at the mean flow velocity) in the mean flow around the trailing edge, as indicated in Figure 2. For the purpose of illustration it will be temporarily assumed (in this section only) that the frequency is sufficiently small that the hydrofoil chord may be regarded as *acoustically compact*. This may or may not be true in practice, but the following discussion will still supply an excellent indication of the relative strengths of these sources.

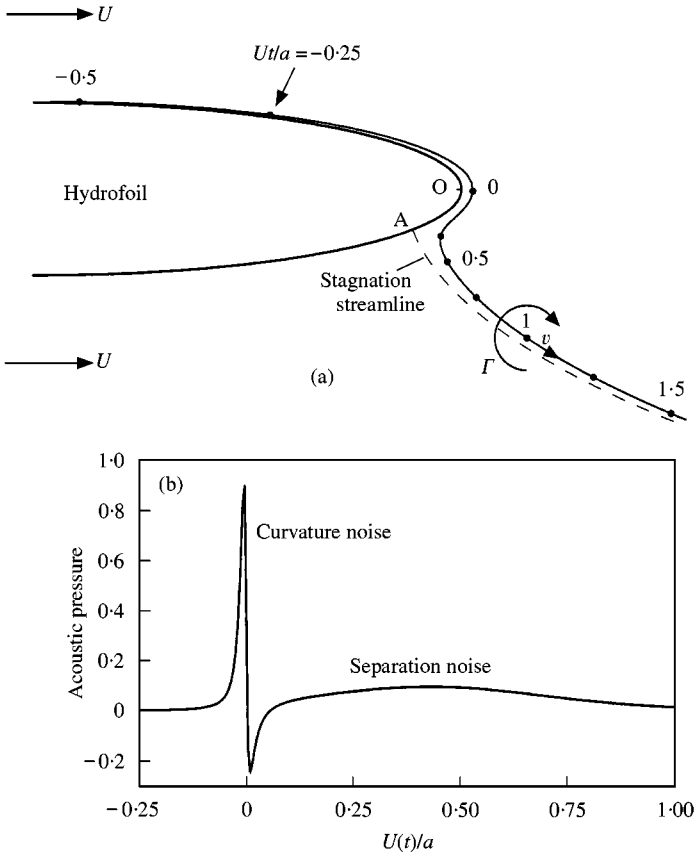


Figure 2. (a) Trajectory of the line vortex (5) around the trailing edge of an elliptic airfoil of semimajor and minor axes $a$, $b$ with $b/a = 0{\cdot}2$, for $U = 2{\cdot}5$ m/s, $a = 1{\cdot}5$ m, $C_L = 3{\cdot}5$. The vortex is released at the midchord position at a standoff distance equal to the nominal boundary layer displacement thickness $\delta_* = 0{\cdot}0024a$. (b) Non-dimensional farfield acoustic pressure $p(\mathbf{x}, t)/[(\rho_0 U^2)(\Gamma L \cos\Theta/c_0 a|\mathbf{x}|)]$ plotted as a function of the retarded time $[t] = t - |\mathbf{x}|/c_0$, showing the "curvature noise" produced when the vortex passes around the trailing edge at O, and the "separation noise" generated near A.

Let $\mathbf{X}_\Gamma(t) = (X_{\Gamma 1}, X_{\Gamma 2})$ denote the position of the vortex in the $x_1x_2$-plane, and write

$$\mathbf{\Omega} = -\Gamma \mathbf{i}_3 \delta(\mathbf{X} - \mathbf{X}_\Gamma(t)), \quad \mathbf{X} = (x_1, x_2), \quad |x_3| < L/2, \tag{5}$$

where $\mathbf{i}_3$ is a unit vector in the spanwise ($x_3$) direction, and $\Gamma > 0$ is the vortex strength (corresponding to circulation in the clockwise sense indicated in the figure). At the "ends" $x_3 = \pm L/2$, the vortex may be assumed to bend down to the surface S or into an upstream direction, in such a manner that end effects may be ignored.

When the hydrofoil is compact the dominant component of the sound generated by the vortex is equivalent to that produced by a dipole source whose strength is equal to the unsteady induced lift, and can be calculated from equation (1) by substituting representation (5) for $\mathbf{\Omega}$ and by using the compact approximation to the Green function, as described in detail in section 3.2 of reference [17]. This calculation yields

$$p(\mathbf{x}, t) \approx \frac{-\rho_0 L \Gamma \cos\Theta}{4\pi c_0 |\mathbf{x}|} \frac{\mathrm{d}}{\mathrm{d}t}[\mathbf{v} \cdot \nabla \Psi], \quad |\mathbf{x}| \to \infty, \tag{6}$$

where the term in the square brackets is evaluated at the retarded position $\mathbf{X}_\Gamma(t - |\mathbf{x}|/c_0)$ of the vortex, $\Theta = \cos^{-1}(x_2/|\mathbf{x}|)$ is the angle between the radiation direction and that of the mean lift, and the function $\Psi(\mathbf{x})$ is determined by the cross-sectional shape of the hydrofoil, and represents physically the stream function of a hypothetical incompressible, irrotational flow past the hydrofoil that has unit speed in the $x_2$ direction at large distances from the hydrofoil. Evidently, sound production by the vortex will be maximal at those locations on its trajectory around the hydrofoil where its acceleration across the streamlines of the hypothetical potential flow is greatest.

Figure 2(b) depicts a typical prediction of equation (6). In performing this calculation, the stream function $\Psi$ and the trajectory of the vortex have been determined by taking the hydrofoil cross-section to be an ellipse of semi-major and minor axes respectively equal to $a$ and $b$ with $b/a = 0{\cdot}2$. The general case in which explicit account is taken of the circular profile of the CC hydrofoil at the trailing edge requires a preliminary numerical calculation to determine $\Psi(\mathbf{x})$, but the rounding has been ignored in evaluating equation (6), because predictions of sound generation by the vortex are only minimally influenced by these geometrical differences when the trajectory and $\Psi$ are *both* approximated in this way.

The trajectory of the vortex $\Gamma$ is shown in Figure 2(a) as a function of $Ut/a$ when the hydrofoil is at zero angle of attack, and the lift produced by the Coanda jet (not shown in the figure) is characterized by a *lift coefficient* $C_L = 3{\cdot}5$. This corresponds to a mean circulation about the hydrofoil equal to $C_L aU$, and the mean flow convecting the vortex around the trailing edge has been calculated using the potential theory of steady flow past the ellipse with this circulation [19]. We have taken $U = 2{\cdot}5$ m/s, and the chord $2a$ to be 3 m. The vortex is released on the suction side of the hydrofoil at the midchord position at a distance $0{\cdot}0024a$ from the surface; this distance is approximately equal to the boundary layer displacement thickness $\delta_*$ when a turbulent boundary layer on S is assumed to start near the leading edge of the hydrofoil. In the figure, the trajectory has been shifted to the right by 2·5% of the semi-major axis $a$ in order to make the vortex path adjacent to the hydrofoil visible.

The non-dimensional acoustic pressure signature

$$\frac{p(\mathbf{x}, t)}{(\rho_0 U^2)(\Gamma L \cos\Theta/c_0 a|\mathbf{x}|)}$$

determined by equation (6) is plotted in Figure 2(b) as a function of the non-dimensional retarded time $U[t]/a$, $[t] = t - |\mathbf{x}|/c_0$ (corresponding to retarded positions shown in Figure 2(a)). A comparison of the figures shows that no sound is produced until the vortex arrives at the point of maximum curvature O. This "curvature noise" pulse has a duration $\sim 0{\cdot}1a/U$ s, corresponding to a minimum principal frequency $\sim 10U/a \approx 16$ Hz. The vortex trajectory separates from the hydrofoil close to the stagnation point A; Figure 2(b) shows that the "separation noise" produced by the vortex is of very low frequency and amplitude. Therefore, this contribution to the overall radiation is henceforth ignored.

## 3. CURVATURE NOISE

### 3.1. CALCULATION OF THE ACOUSTIC PRESSURE

In this section, the frequency spectrum of the curvature noise generated by turbulence in the boundary layer flow over the rounded edge O of the hydrofoil is determined from equation (3), by expressing the upwash velocity $v$ in terms of an empirical model of the local turbulent boundary layer wall pressure. At high frequencies it is not permissible to assume

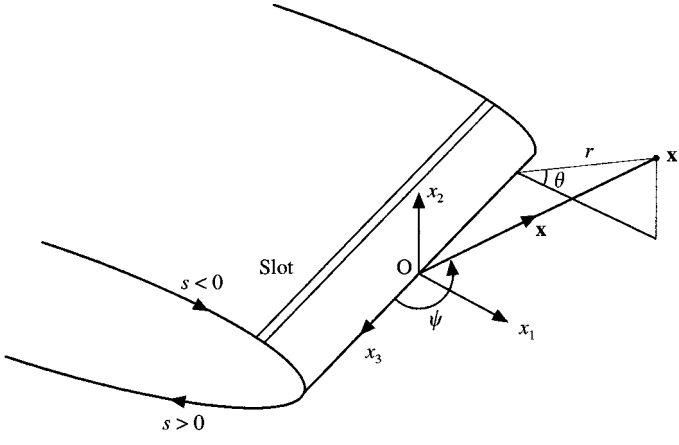


Figure 3. Co-ordinates used to define the farfield observer position **x**.

(as in section 2.2) that the chord $2a$ is acoustically compact. Since these higher frequency components are probably of more interest in applications, detailed calculations will be reported only for the case of non-compact chord. Low-frequency estimates can subsequently be corrected, where necessary, for the influence of finite chord, by applying the interpolation formula given in section 4.2 of reference [24].

Take the origin of co-ordinates at a point O on the trailing edge of the hydrofoil (see Figure 3), and consider the Fourier component $p(\mathbf{x}, \omega)\mathrm{e}^{-\mathrm{i}\omega t}$ of the farfield acoustic pressure $p(\mathbf{x}, t)$. When the chord is non-compact it is shown in reference [18] that the frequency domain form of equation (3) is

$$p(\mathbf{x}, \omega) \approx \frac{\rho_0 \omega \sqrt{\mathrm{i}\kappa_0}\sin^{1/2}\psi \sin(\theta/2)}{\pi\sqrt{2\pi}|\mathbf{x}|} \oint_S \Phi^*(\mathbf{y}) v_n(\mathbf{y}, \omega)\mathrm{e}^{\mathrm{i}\kappa_o|\mathbf{x} - \mathrm{i}_3 y_3|}\,\mathrm{d}S(\mathbf{y}), \quad |\mathbf{x}| \to \infty, \tag{7}$$

where $\kappa_0 = \omega/c_0$ is the acoustic wavenumber and $v_n(\mathbf{y}, \omega) = 1/2\pi\int_{-\infty}^{\infty} v_n(\mathbf{y}, t)\mathrm{e}^{\mathrm{i}\omega t}\,\mathrm{d}t$. The function $\Phi^*(\mathbf{y})$ is a solution of Laplace's equation whose functional form is determined by the geometry of the slot region; the velocity $v_n$ characterizes the turbulence velocity that would exist in the absence of the slot but with the same boundary layer structure. The integral accordingly represents the production of sound by the scattering (or "diffraction") of this velocity by the slot. The gradient of $\Phi^*(\mathbf{y})$ is the velocity of a potential flow around the trailing edge (in the *anticlockwise* sense in Figure 1), and it is normalized such that

$$\Phi^*(\mathbf{y}) \to \mathrm{Re}\{-\mathrm{i}z^{1/2}\} \quad \text{or } |z| \gg \Re, \quad z = y_1 + \mathrm{i}y_2. \tag{8}$$

In terms of polar co-ordinates $(y_1, y_2) = r'(\cos\theta', \sin\theta')$, the limiting form $\mathrm{Re}\{-\mathrm{i}z^{1/2}\} = \sqrt{r'}\sin(\theta'/2)$; this is the potential for anticlockwise irrotational flow around the edge of the half-plane $y_1 < 0$, $y_2 = 0$. The angles $\theta$, $\psi$ define the farfield radiation direction $\mathbf{x}/|\mathbf{x}|$, as indicated in Figure 3, where $(x_1, x_2) = r(\cos\theta, \sin\theta)$ and $\psi$ is the angle between the spanwise direction (the $x_3$-axis) and the radiation direction.

To evaluate the integral in equation (7) we put $\mathrm{d}S = \mathrm{d}s\,\mathrm{d}y_3$, where $s$ is the curvilinear distance from O measured on S in the $x_1x_2$-plane, as indicated in Figure 3. If we also introduce the Fourier integral representation on S,

$$v_n(\mathbf{y}, \omega) = \iint_{-\infty}^{\infty} v_n(k, k_3, \omega)\,\mathrm{e}^{\mathrm{i}(ks + k_3 y_3)}\,\mathrm{d}k\,\mathrm{d}k_3, \tag{9}$$

then, as $|\mathbf{x}| \to \infty$,

$$\oint_S \Phi^*(\mathbf{y}) v_n(\mathbf{y}, \omega) e^{i\kappa_0|\mathbf{x} - \mathbf{i}_3 y_3|} dS(\mathbf{y}) = 2\pi e^{i\kappa_0|\mathbf{x}|} \int\int_{-\infty}^{\infty} v_n(k, \kappa_0 \cos\psi, \omega)\, \Phi^*(s)\, e^{iks}\, ds\, dk, \qquad (10)$$

where $\phi^*(\mathbf{y}) \equiv \Phi^*(s)$ on S. The principal contribution to the $s$-integral is from the immediate vicinity of $s = 0$, and it is only the behavior of $\Phi^*(s)$ near this point that is important. Therefore, without loss of accuracy $\Phi^*(s)$ can be approximated by the corresponding potential $\Phi_0^*(s)$, say, of flow past a parabolic edge whose minimum radius of curvature (at $s = 0$) is $\mathfrak{R}$, i.e., by

$$\Phi_0^*(\mathbf{y}) = \sqrt{(y_1 + \mathfrak{R}/2)^2 + y_2^2}\, \sin\left(\frac{1}{2}\tan^{-1}\left[\frac{y_2}{\sqrt{(y_1 + \mathfrak{R}/2)^2 + y_2^2}}\right]\right). \qquad (11)$$

In a typical application $\mathfrak{R} \sim 0{\cdot}08a$, $a = 1{\cdot}5$ m, and the hydrodynamic wavenumber $k \sim \omega/U_0$ where $U_0 \sim 10$ m/s. Thus, $k\mathfrak{R} \sim 0{\cdot}08\omega a/U_0 > 1$ when the frequency $f = \omega/2\pi$ satisfies

$$f > \frac{U_0}{0{\cdot}5a} \sim 13 \text{ Hz} \quad \text{for} \quad a = 1{\cdot}5 \text{ m}.$$

It may therefore be assumed in evaluating the integration with respect to $s$ in equation (10) that $k\mathfrak{R} \gg 1$ for all acoustic frequencies of interest. In this asymptotic limit, we find

$$\int_{-\infty}^{\infty} \Phi_0^*(s) e^{iks}\, ds \approx \frac{-1}{k}\sqrt{\frac{\pi}{|k|}}\, e^{-|k|\mathfrak{R}/2}$$

and equation (7) becomes

$$p(\mathbf{x}, \omega) \approx \frac{-\rho_0\omega\sqrt{i\kappa_0}\, \sin^{1/2}\psi \sin(\theta/2) e^{i\kappa_0|\mathbf{x}|}}{\sqrt{2}|\mathbf{x}|} \int_{-\infty}^{\infty} \frac{v_n(k, \kappa_0, \cos\psi, \omega) e^{-|k|\mathfrak{R}/2}}{k\sqrt{|k|}}\, dk, \quad |\mathbf{x}| \to \infty. \qquad (12)$$

Now when $k\mathfrak{R} \gg 1$, the hydrodynamic length scale is much smaller than the surface radius of curvature, and we can estimate the value of $v_n(k, \kappa_0 \cos\psi, \omega)$ in terms of the boundary layer turbulence surface pressure fluctuations by assuming the surface S to be locally *flat* (on the scale of $1/k$). The pressure on S may be imagined to have two components: the first is the "incident" pressure $p_I$ produced by the turbulence when its interaction with S is ignored; this satisfies $\rho_0 \partial \mathbf{v}/\partial t = -\nabla p_I$ on S, where $\mathbf{v}$ is the upwash velocity. The second is the pressure $p_R$ "reflected" from S. On a locally flat surface S: $p_I = p_R$, where the two pressures combine to form the "blocked surface pressure" $p_s(k, \kappa_0 \cos\psi, \omega)$, say. Because these pressures must vary like $e^{i(ks + y_3\kappa_0 \cos\psi)}$ on S, and $\kappa_0 \ll k \sim \omega/U_0$ in very low Mach number flows, the incident pressure must be proportional to $e^{|k|y_n}$ very close to S, where $y_n$ is measured outward in the normal direction from S (i.e., $p_I$ must decay with distance "into" S). Therefore (because $\rho_0 \partial v_n/\partial t = -\partial p_I/\partial y_n$ on S), we can write

$$v_n(k, \kappa_0 \cos\psi, \omega) = \frac{-i|k| p_I(k, \kappa_0 \cos\psi, \omega)}{\rho_0\omega} \equiv \frac{-i|k| p_s(k, \kappa_0 \cos\psi, \omega)}{2\rho_0\omega}. \qquad (13)$$

This relation permits the upwash velocity to be expressed locally in terms of measured values (or an empirical model) of the blocked surface pressure.

When this is inserted into equation (12), and the result is summed over all frequencies $\omega$, the farfield acoustic pressure is obtained in the form

$$p(\mathbf{x}, t) \approx \frac{-\sin^{1/2}\psi \sin(\theta/2)}{2\sqrt{2c_0}|\mathbf{x}|} \int\int_{-\infty}^{\infty} \frac{\sqrt{\omega}\,\mathrm{sgn}(k) p_s(k, \kappa_0 \cos\psi, \omega) \mathrm{e}^{-|k|\Re/2 - \mathrm{i}(\omega[t] + \pi/4)}}{|k|^{1/2}} \mathrm{d}k\,\mathrm{d}\omega,$$

$$|\mathbf{x}| \to \infty. \tag{14}$$

### 3.2. CURVATURE NOISE FREQUENCY SPECTRUM

Let a finite section $-\frac{1}{2}L < x_3 < \frac{1}{2}L$ of the airfoil span, of width $L \gg \delta$ = thickness of the turbulent boundary layer at O, be wetted by the turbulent flow. When the flow is statistically stationary in time the blocked surface pressure $p_s$ satisfies

$$\langle p_s(k, k_3, \omega) p_s^*(k', k_3, \omega') \rangle \approx \frac{L}{2\pi} \delta(\omega - \omega') \delta(k - k') P(k, k_3, \omega), \quad L \gg \delta, \tag{15}$$

where the angle brackets $\langle\ \rangle$ represent an ensemble average, the asterisk denotes complex conjugate, and $P(\mathbf{k}, \omega)$ is the blocked surface pressure wavenumber–frequency spectrum [17, 25].

Then if the *one-sided* acoustic pressure frequency spectrum of the curvature noise is denoted by $\Phi_{\mathrm{O}}(\mathbf{x}, \omega)$, such that

$$\langle p^2(\mathbf{x}, t) \rangle = \int_0^{\infty} \Phi_{\mathrm{O}}(\mathbf{x}, \omega)\,\mathrm{d}\omega, \quad |\mathbf{x}| \to \infty, \tag{16}$$

equations (14) and (15) supply

$$\Phi_{\mathrm{O}}(\mathbf{x}, \omega) \approx \frac{\omega L \sin^2(\theta/2) \sin\psi}{8\pi c_0 |\mathbf{x}|^2} \int_{-\infty}^{\infty} \frac{\mathrm{e}^{-|k|\Re}}{|k|} P(k, \kappa_0 \cos\psi, \omega)\,\mathrm{d}k, \quad |\mathbf{x}| \to \infty. \tag{17}$$

To simplify this result we suppose that $P(k, k_3, \omega)$ is similar in form to the wall-pressure spectrum for a flat wall boundary layer [17, 25]. Thus, if $U_0$ is the mean flow speed *parallel* to S just outside the boundary layer at O, $P(k, k_3, \omega)$ will have a very large maximum in the vicinity of $k = \omega/U_{\mathrm{oc}}$, $k_3 = 0$, where $U_{\mathrm{oc}} \sim 0{\cdot}7U_{\mathrm{o}}$ is a boundary layer turbulence convection velocity. Now $\kappa_0\delta \ll 1$, because the March number of the flow is infinitesimal; the integral in equation (17) can therefore be approximated by setting $\kappa_0 = 0$ in the argument of $P(k, \kappa_0 \cos\psi, \omega)$ and replacing the factor $\mathrm{e}^{-|k|\Re}/|k|$ by its value at $k = \omega/U_{\mathrm{oc}}$, i.e.,

$$\int_{-\infty}^{\infty} \frac{\mathrm{e}^{-|k|\Re}}{|k|} P(k, \kappa_0 \cos\psi, \omega)\,\mathrm{d}k \approx \frac{\ell_3}{\pi} \Phi_{pp}(\omega) \frac{\mathrm{e}^{-\omega\Re/U_{\mathrm{oc}}}}{(\omega/U_{\mathrm{oc}})}, \quad \omega > 0, \tag{18}$$

where $\ell_3 \approx U_{\mathrm{o}}/\omega$ is the Corcos [26] spanwise correlation length, and $\Phi_{pp}(\omega)$ is the frequency spectrum of the blocked wall pressure. If we adopt Chase's [25] collation of experimental data, we can model the wall-pressure frequency spectrum by

$$\frac{(U_{\mathrm{o}}/\delta_*)\Phi_{pp}(\omega)}{(\rho_0 v_*^2)^2} = \frac{(\omega\delta_*/U_{\mathrm{o}})^2}{[(\omega\delta_*/U_{\mathrm{o}})^2 + \alpha_p^2]^{3/2}}, \quad \alpha_p = 0{\cdot}12, \tag{19}$$

where $v_*$ is the boundary layer friction velocity at O [27].

Thus, the curvature noise spectrum (17) may finally be cast in the form

$$\frac{(U/a)\Phi_{\rm O}(\mathbf{x},\omega)}{(\rho_0U^2)^2(La/|\mathbf{x}|^2)M\sin^2(\theta/2)\sin\psi}\approx\frac{0{\cdot}7}{8\pi^2}\left(\frac{\delta_*}{a}\right)^2\left(\frac{v_*}{U}\right)^4\frac{(\omega\delta_*/U_{\rm o})\mathrm{e}^{-\omega\Re/U_{\rm oc}}}{[(\omega\delta_*/U_{\rm o})^2+\alpha_p^2]^{3/2}},\tag{20}$$

where $M=U/c_0$, and where $v_*\sim 0{\cdot}035U_{\rm o}$, $\delta_*$ are the local values of the friction velocity and boundary layer displacement thickness at O.

## 4. SLOT NOISE

### 4.1. INTEGRAL REPRESENTATION OF THE SOUND

Sound is generated at the slot by the "scattering" by the slot lip of the evanescent (or hydrodynamic) pressure fluctuations produced by turbulence in the exterior mean flow boundary layer on S and by any turbulence within the high speed Coanda jet. To estimate the corresponding contributions to the farfield acoustic spectrum the thickness of the slot lip will be assumed to be constant and equal to $\Delta$, and the influence of wall curvature in the immediate neighborhood of the slot will be ignored; the latter assumption is justified by the observation that the length scales of the dominant slot sources must be comparable to the slot width $h$ which, being typically smaller than about $10^{-2}a$, is itself very much smaller than the local radius of curvature of S. This simplified analytical model of the Coanda slot geometry is shown in Figure 4(a); for the purpose of calculating the interaction

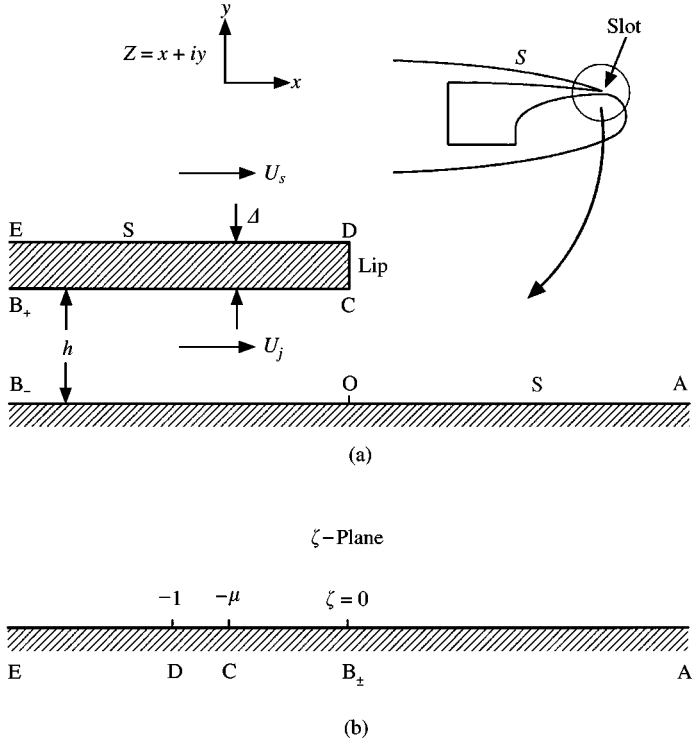


Figure 4. (a) Local geometry in the $Z$-plane of the Coanda jet slot and lip, with Coanda jet velocity $U_j$ and exterior mean flow speed $U_s$; (b) image in $\mathrm{Im}\,\zeta>0$ of the fluid region (exterior to the lip) in the upper half of the $Z$-plane.

of the flow with the lip CD, the slot-duct width is taken to be uniform and equal to $h$. In the figure the "upper" side ED represents the surface S of the hydrofoil just upstream of the slot; the end A of the lower wall $B_-A$ is the continuation of S downstream of the slot; the upstream interior ends $B_\pm$ of the duct would eventually diverge into the jet plenum, but the precise shape of the duct several duct widths $h$ upstream of C does not materially affect predictions of the sound.

The sound produced by the interaction of the exterior boundary layer and the Coanda jet turbulence with the lip can be evaluated from the general formula (7), with the surface integral confined to the exterior and interior surfaces $EDCB_+$ of the slot lip, and to the wall $B_-A$. To do this we must determine the form of the potential function $\Phi^*(\mathbf{y})$ near the slot. This function satisfies $\Phi^*(\mathbf{y}) \sim \Phi_o^*(\mathbf{y})$ (given by equation (11)) at distances from the slot greatly exceeding the slot width $h$. Suppose the outer corner D of the lip (which is parallel to the span of the hydrofoil) is at $\mathbf{X}_s = (X_{s1}, X_{s2})$, then near the slot we can write

$$\Phi^*(\mathbf{y}) = \Phi_o^*(\mathbf{X}_s) - \Phi_o^{*\prime}\varphi^*(\mathbf{y}), \quad \text{where } \Phi_o^{*\prime} = |\nabla\Phi_o^*(\mathbf{X}_s)|. \tag{21}$$

In the formula $\Phi_o^{*\prime}$ represents the magnitude of the potential flow velocity at $\mathbf{X}_s$ defined by the velocity potential $\Phi_o^*(\mathbf{y})$ when the presence of the slot is ignored. Very close to the hydrofoil, this velocity is parallel to the nominal surface of the hydrofoil, so that in equation (21) the function $\varphi^*(\mathbf{y})$ must represent the distortion of this hypothetical flow by the presence of the slot. The behavior of $\varphi^*(\mathbf{y})$ can be specified precisely in terms of local co-ordinates $(x, y)$ in the streamwise $x_1x_2$-plane, with origin at O in Figure 4(a), the positive $x$-axis lying along OA, and with $y$ measured outwards into the fluid from O, such that the inner and outer corners of the lip C and D are, respectively, at $(0, h)$ and $(0, h + \Delta)$. In other words, in the vicinity of the slot we use the local co-ordinate system $\mathbf{y} = (x, y, y_3)$. Then in the exterior region, upstream and downstream of the slot in Figure 4(a), the velocity $\nabla\varphi^*(\mathbf{y})$ must represent flow at *unit speed in the positive* $x$ direction.

The functional form of $\varphi^*(\mathbf{y}) \equiv \varphi^*(x, y)$ is found by setting $Z = x + iy$, and mapping the upper half of the complex $Z$-plane exterior to the semi-infinite rectangular domain $EDCB_+$ (i.e., exterior to the slot lip of Figure 4(a)) onto the upper half of the $\zeta$-plane by means of the Schwarz–Christoffel transformation [28]

$$\frac{Z}{h} = \frac{1}{\pi\sqrt{\mu}}\{(\zeta+1)^{1/2}(\zeta+\mu)^{1/2} + (1+\mu)\ln[(\zeta+1)^{1/2} + (\zeta+\mu)^{1/2}]$$

$$- 2\sqrt{\mu}\ln[\sqrt{\mu}(\zeta+1)^{1/2} + (\zeta+\mu)^{1/2}] + \sqrt{\mu}\ln\zeta - (1-\sqrt{\mu})^2\ln\sqrt{1-\mu}\},$$

$$0 < \mu < 1, \quad \operatorname{Im}\zeta > 0. \tag{22}$$

The points E, D, C, $B_\pm$, A all map onto the real axis in the $\zeta$-plane in the manner indicated in Figure 4(b): the lip $EDCB_+$ maps into the negative real axis $(-\infty, 0)$, and lower wall $B_-A$ maps onto the positive real axis. The value of $\mu$ is given in terms of the thickness $\Delta$ of the lip by

$$\mu = 1/\left[1 + \Delta/h + \sqrt{(1+\Delta/h)^2 - 1}\,\right]^2. \tag{23}$$

The image in the $\zeta$-plane of the flow past the slot represented by the potential function $\varphi^*(\mathbf{y}) \equiv \varphi^*(x, y)$ is a flow at uniform speed in the positive direction of the real $\zeta$-axis, whose complex potential is therefore a linear function of $\zeta$. According to equation (22), $Z \sim h\zeta/\pi\sqrt{\mu}$ at large distances from the slot in the exterior region, so that unit speed at

large distances from the slot in the $Z$-plane is obtained by taking

$$\varphi^*(x, y) = \mathrm{Re}\left[\frac{h}{\pi\sqrt{\mu}}(\zeta + 1)\right], \tag{24}$$

where the constant "1" is included to ensure that $\varphi^*$ vanishes at the corner D of the lip. By evaluating $\Phi_o^{*\prime} = |\nabla\Phi_o^*(\mathbf{X}_s)|$ from definition (11), we may now cast the local representation (21) in the form

$$\Phi^*(\mathbf{y}) = \Phi_o^*(\mathbf{X}_s) + \alpha\,\mathrm{Re}(\zeta(Z) + 1), \quad \text{where } \alpha = \frac{-h}{2\pi\sqrt{\mu}[(X_{s1} + \Re/2)^2 + X_{s2}^2]^{1/4}}. \tag{25}$$

### 4.2. PASSIVE SLOT NOISE GENERATED BY THE EXTERNAL BOUNDARY LAYER

"Passive" slot noise is produced by the diffraction of the exterior mean flow boundary layer turbulence wall pressure on S by the lip of the jet slot. It is determined by the contribution to integral (7) from the vicinity of the slot, with $v_n$ calculated from the properties of the external boundary layer flow impinging on the slot from upstream. To do this it is assumed that in the neighborhood of the slot lip all of the turbulence in the exterior boundary layer lies in the region $y \geqslant h + \Delta$ *above* the lip. Then in the region $y < h + \Delta$, each frequency component $p_I(\mathbf{y}, \omega)$ of the hydrodynamic pressure $p_I(\mathbf{y}, t)$ that would be generated by the boundary layer turbulence when diffraction at the surface S is ignored can be cast in the form

$$p_I(\mathbf{y}, \omega) = \iint_{-\infty}^{\infty} p_I(k, k_3, \omega)\,\mathrm{e}^{\mathrm{i}(kx + k_3 y_3) - (h + \Delta - y)\sqrt{k^2 + k_3^2}}\,\mathrm{d}k\,\mathrm{d}k_3, \quad y < h + \Delta, \tag{26}$$

where the exponential factor $\mathrm{e}^{-(h+\Delta-y)\sqrt{k^2+k_3^2}}$ accounts for the "evanescent" decrease in amplitude of the induced pressure with distance $h + \Delta - y$ "below" the boundary layer. According to this definition, $p_s(k, k_3, \omega) = 2p_I(k, k_3, \omega)$ may be interpreted as the blocked pressure on S upstream of the outer corner D of the lip. The Fourier transform $\mathbf{v}(\mathbf{y}, \omega)$ of the upwash velocity on S may now be calculated from

$$\mathbf{v}(\mathbf{y}, \omega) = \frac{1}{\mathrm{i}\rho_0\omega}\,\nabla p_I(\mathbf{y}, \omega). \tag{27}$$

Now $\mathrm{d}S(\mathbf{y}) = \mathrm{d}s\,\mathrm{d}y_3$ in the integral $\oint_S \Phi^*(\mathbf{y}) v_n(\mathbf{y}, \omega)\mathrm{e}^{\mathrm{i}\kappa_0|\mathbf{x} - \mathbf{i}_3 y_3|}\,\mathrm{d}S(\mathbf{y})$ of equation (7), where $s$ is the curvilinear distance on S in the $xy$-plane. By writing $Z = x + \mathrm{i}y$ and noting that

$$\int_{-\infty}^{\infty} \mathrm{e}^{\mathrm{i}\{\kappa_0|\mathbf{x} - \mathbf{i}_3 y_3| + k_3 y_3\}}\,\mathrm{d}y_3 = 2\pi\delta(k_3 - \kappa_0\cos\psi)\mathrm{e}^{\mathrm{i}\kappa_0|\mathbf{x}|}, \quad |\mathbf{x}| \to \infty,$$

we find

$$\oint_S \Phi^*(\mathbf{y}) v_n(\mathbf{y}, \omega)\mathrm{e}^{\mathrm{i}\kappa_0|\mathbf{x} - \mathbf{i}_3 y_3|}\,\mathrm{d}S(\mathbf{y}) = \frac{\alpha\pi\mathrm{e}^{\mathrm{i}\kappa_0|\mathbf{x}|}}{\rho_0\omega}\int_{-\infty}^{\infty} \mathrm{sgn}(k)\, p_s(k, \kappa_0\cos\psi, \omega)\mathscr{I}_S(k)\,\mathrm{d}k, \tag{28}$$

where

$$\mathscr{I}_S(k) = \text{c.c.}\left\{\frac{-\mathrm{i}k\mathrm{e}^{-(h+\Delta)|k|}}{\alpha}\oint_\gamma \Phi^*(\mathbf{y})\mathrm{e}^{-\mathrm{i}kZ}\,\mathrm{d}Z\right\}, \quad k>0$$

$$= \text{c.c.}\{\mathscr{I}_S(-k)\}, \quad k<0, \tag{29}$$

and the notation c.c $\{\cdot\}$ implies the complex conjugate of the quantity in the brace brackets. The integral defining $\mathscr{I}_S$ is taken over the piecewise rectilinear contour $\gamma = \mathrm{AB}_-\mathrm{B}_+\mathrm{CDE}$ in the $Z$-plane of Figure 4(a), starting at A and ending at E; and we have made the low Mach number approximation $\mathrm{e}^{-(h+\Delta)\sqrt{k^2+k_0^2\cos^2\psi}} \approx \mathrm{e}^{-|k|(h+\Delta)}$, which is applicable in the hydrodynamic domain $k \sim \omega/U_s \gg \omega/c_0$ occupied by the boundary layer pressure sources.

Only those contributions to the integral $\mathscr{I}_S$ from the neighborhood of the mouth of the slot are relevant, since turbulence sources may be assumed to be absent very far upstream, and to die out (i.e., become incoherent with the sources near the slot) at large distances downstream. This means, that when using approximation (25) for $\Phi^*(\mathbf{y})$ (which is valid only close to the slot) to evaluate $\mathscr{I}_S$, it is permissible to secure convergence of the integrals by integrating by parts and formally discarding contributions from $Z = +\infty$ and $-\infty + \mathrm{i}(h+\Delta)$. By noting that $\zeta$ is real on $\gamma$, we then find, integrating by parts once,

$$\mathscr{I}_S(k) = c.c.\left\{-\mathrm{e}^{-(h+\Delta)|k|}\oint_\gamma \frac{\mathrm{d}\zeta}{\mathrm{d}Z}\mathrm{e}^{-\mathrm{i}kZ}\,\mathrm{d}Z\right\} = \text{c.c.}\left\{\mathrm{e}^{-(k+\Delta)|k|}\int_{-\infty}^{\infty}\mathrm{e}^{-\mathrm{i}kZ(\zeta)}\,\mathrm{d}\zeta\right\}, \quad k>0. \tag{30}$$

The final integration with respect to $\zeta$ is taken along the real axis, passing just above the integrable singularities of $Z(\zeta)$.

Hence, collecting together these results for equation (28) and substituting into equation (7) we finally obtain, after summing over all frequency components, the passive slot noise acoustic pressure:

$$p(\mathbf{x},t) \approx \frac{-h\sin^{1/2}\psi\sin(\theta/2)}{(2\pi)^{3/2}\sqrt{\mu c_0}|\mathbf{x}|[(X_{s1}+\Re/2)^2+X_{s2}^2]^{1/4}}\iint_{-\infty}^{\infty}\sqrt{\mathrm{i}\omega}\,\mathrm{sgn}(k)p_s(k,\kappa_0\cos\psi,\omega)$$

$$\times\mathscr{I}_S(k)\mathrm{e}^{-\mathrm{i}\omega[t]}\,\mathrm{d}k\,\mathrm{d}\omega, \quad |\mathbf{x}|\to\infty. \tag{31}$$

This can be used to calculate the corresponding one-sided acoustic pressure spectrum $\Phi_S(\mathbf{x},\omega)$ of the passive slot noise (defined as in equation (16)):

$$\Phi_S(\mathbf{x},\omega) \approx \frac{\omega L h^2\sin^2(\theta/2)\sin\psi}{8\pi^4\mu c_o[(X_{s1}+\Re/2)^2+X_{s2}^2]^{1/2}|\mathbf{x}|^2}\int_{-\infty}^{\infty}|\mathscr{I}_S(k)|^2P(k,\kappa_0\cos\psi,\omega)\,\mathrm{d}k, \quad |\mathbf{x}|\to\infty, \tag{32}$$

where $P(k,k_3,\omega)$ is the exterior boundary layer blocked surface pressure wavenumber-frequency spectrum just upstream of the slot. When $kh \gg 1$ this formula reduces in form to that describing the production of sound by turbulent boundary layer flow over a "rectangular" trailing edge of thickness $\Delta$ when the flow is assumed to separate at the corner adjacent to the boundary layer [17]. In this limit, the interaction of the

exterior boundary layer turbulence with the "image" of the lip in the inner wall B_A of Figure 4(a) becomes negligible.

Numerical estimates can be made by evaluating the remaining integral in equation (32) by an approximation of the type used in equation (18), together with a corresponding formula (19) for the local blocked surface pressure frequency spectrum on the hydrofoil just upstream of the slot. The result can be expressed in the following form analogous to the curvature noise spectrum (20):

$$\frac{(U/a)\Phi_S(\mathbf{x},\omega)}{(\rho_0 U^2)^2(La/|\mathbf{x}|^2)M\sin^2(\theta/2)\sin\psi}$$

$$\approx \frac{1}{8\pi^5}\frac{h}{[(X_{s1}+\Re/2)^2+X_{s2}^2]^{1/2}}\left(\frac{h\delta_*}{a^2}\right)\left(\frac{v_*}{U}\right)^4\frac{(\omega\delta_*/U_s)^2|\mathscr{I}_S(\omega/U_{sc})|^2}{[(\omega\delta_*/U_s)^2+\alpha_p^2]^{3/2}}, \tag{33}$$

where $U_{sc}\approx 0{\cdot}7U_s$, $U_s$ being the mean flow speed indicated in Figure 4(a) just outside the exterior boundary layer above the slot, and $\delta_*$ and $v_*$ are local values of the boundary layer displcement thickness and friction velocity.

In general $|\mathscr{I}_S(\omega/U_{sc})|^2$ must be evaluated numerically from definition (30). Since the integral in equation (30) is dominated by contributions from the neighborhood of the lip, numerical evaluation is facilitated (for $k>0$) by first deforming the contour in the $\zeta$-plane onto the piecewise rectilinear path joining the points $\zeta = 1-\mathrm{i}\infty, -1, 0, -\mathrm{i}\infty$, where the section along the real axis between $\zeta=-1, 0$ passes *above* the singularities of $Z(\zeta)$. On this contour the integrand is exponentially small at the two extremes where $\zeta\to-\mathrm{i}\infty$. The following two limiting cases can be evaluated explicitly:

$$|\mathscr{I}_S(k)|^2=\begin{cases} 3\Gamma^2\left(\frac{5}{3}\right)\Big/\left[\frac{2|k|h\sqrt{1/\mu-1}}{3\pi}\right]^{4/3}, & |k|\Delta\gg 1,\quad \Delta\neq 0;\\ \frac{2\pi^2}{|k|h}(1-\mathrm{e}^{-2|k|h}), & \Delta=0. \end{cases} \tag{34}$$

These formulae, respectively, define the high-frequency behavior when the lip thickness $\Delta\neq 0$, and the exact behavior for all frequencies when $\Delta=0$ (i.e., when $\Delta\ll h$).

### 4.3. SLOT NOISE GENERATED BY THE COANDA JET

In typical underwater applications, the Coanda jet Reynolds number $U_j h/\nu\sim 10^5$ ($\nu\sim 10^{-6}\,\mathrm{m}^2/\mathrm{s}$ being the kinematic viscosity of water). This would normally imply that the jet flow from the slot is fully turbulent. However, the exit flow from the plenum converges towards the slot thereby inhibiting instability and the onset of turbulence, so that some care must be exercised in estimating the turbulence properties of the jet. In undersea applications, fouling of interior surfaces may be a source of turbulence.

By symmetry it may be assumed that the blocked surface pressure $p_s$ produced by the turbulent jet on the upper and lower slot duct walls are statistically the same. Then, to evaluate the surface integral $\oint\Phi^*(\mathbf{y})v_n(\mathbf{y},\omega)\mathrm{e}^{\mathrm{i}\kappa_0|\mathbf{x}-\mathbf{i}_3 y_3|}\,\mathrm{d}S(\mathbf{y})$ of equation (7) by the procedure

described above, we can take the "incident" hydrodynamic pressure $p_I(\mathbf{y}, \omega)$ to be given by

$$p_I(\mathbf{y}, \omega) = \iint_{-\infty}^{\infty} p_I(k, k_3, \omega)\, \mathrm{e}^{\mathrm{i}(kx + k_3 y_3) - (y-h)\sqrt{k^2 + k_3^2}}\, \mathrm{d}k\, \mathrm{d}k_3, \quad y \geqslant h \text{ on } B_+\mathrm{CDE},$$

$$= \iint_{-\infty}^{\infty} p_I(k, k_3, \omega)\, \mathrm{e}^{\mathrm{i}(kx + k_3 y_3) + y\sqrt{k^2 + k_3^2}}\, \mathrm{d}k\, \mathrm{d}k_3, \quad y \leqslant 0 \text{ on } \mathrm{B}_-\mathrm{A}, \tag{35}$$

where in these two formulae, $p_I(k, k_3, \omega)$ respectively represents the Fourier transform of the incident pressure generated by the jet turbulence on $\mathrm{B}_+\mathrm{C}$ and $\mathrm{B}_-\mathrm{A}$. In each case, the upwash velocity is calculated from equation (27). The radiated pressures may now be calculated by the method used in section 4.2 for the passive slot noise. In doing this, however, it should be noted that the wall pressures on the upper and lower slot duct walls will normally be *statistically independent* except at very low frequencies. The net acoustic pressure spectrum will therefore be equal to the sum of the separate spectra generated by the upper and lower Coanda jet boundary layers.

In the acoustic far field we find

$$p_{\pm}(\mathbf{x}, t) \approx \frac{\pm\, h \sin^{1/2}\psi \sin(\theta/2)}{(2\pi)^{3/2}\sqrt{\mu c_0}\,|\mathbf{x}|[(X_{s1} + \Re/2)^2 + X_{s2}^2]^{1/4}}$$

$$\times \int_{-\infty}^{\infty} \sqrt{\mathrm{i}\omega}\, \mathrm{sgn}(k)\, p_s(k, \kappa_0 \cos\psi, \omega)\, \mathscr{I}_{\pm}(k)\, \mathrm{e}^{-\mathrm{i}\omega[t]}\, \mathrm{d}k\, \mathrm{d}\omega, \quad |\mathbf{x}| \to \infty, \tag{36}$$

where $p_{\pm}(\mathbf{x}, t)$ denotes the acoustic pressure respectively attributable to the upper/lower boundary layers of the Coanda jet, and

$$\mathscr{I}_+(k) = \frac{\mathrm{i}k\mathrm{e}^{|k|h}}{\alpha} \oint_{B_+}^{E} \Phi^*(\mathbf{y})\mathrm{e}^{\mathrm{i}kZ}\, \mathrm{d}Z \equiv \mathrm{e}^{|k|h} \int_{-\infty}^{0} \mathrm{e}^{\mathrm{i}kZ(\zeta)}\, \mathrm{d}\zeta, \quad k > 0,$$

$$= \text{c.c.}\{\mathscr{I}_+(-k)\}, \quad k < 0, \tag{37}$$

$$\mathscr{I}_-(k) = \text{c.c.}\left\{\frac{-\mathrm{i}k}{\alpha} \oint_{A}^{B_-} \Phi^*(\mathbf{y})\mathrm{e}^{-\mathrm{i}kZ}\, \mathrm{d}Z\right\} \equiv \text{c.c.}\left\{\int_0^{\infty} \mathrm{e}^{-\mathrm{i}kZ(\zeta)}\, \mathrm{d}\zeta\right\}, \quad k > 0,$$

$$= \text{c.c.}\{\mathscr{I}_-(-k)\}, \quad k < 0. \tag{38}$$

The corresponding one-sided acoustic pressure spectra $\Phi_J^{\pm}(\mathbf{x}, \omega)$ are given by

$$\Phi_J^{\pm}(\mathbf{x}, \omega) \approx \frac{\omega L h^2 \sin^2(\theta/2)\sin\psi}{8\pi^4 \mu c_0 [(X_{s1} + \Re/2)^2 + X_{s2}^2]^{2/1}|\mathbf{x}|^2} \int_{-\infty}^{\infty} |\mathscr{I}_{\pm}(k)|^2 P(k, \kappa_0 \cos\psi, \omega)\, \mathrm{d}k,$$

$$|\mathbf{x}| \to \infty, \tag{39}$$

where $P(k, k_3, \omega)$ is the blocked pressure wavenumber-frequency spectrum for the jet, assumed to be the same on the upper and lower walls of the jet slot. The remaining wavenumber integral can be approximated as previously, by expanding about the peak of $P(k, \kappa_0 \cos\psi, \omega) \approx P(k, 0, \omega)$ at $k = \omega/U_{jc}$ (where $U_{jc} \approx 0{\cdot}7U_j$). Using the corresponding

representation (19) of the blocked pressure frequency spectrum, we then find

$$\frac{(U/a)\Phi_J^{\pm}(\mathbf{x},\omega)}{(\rho_0 U^2)^2(La/|\mathbf{x}|^2)M\sin^2(\theta/2)\sin\psi}$$

$$\approx \frac{1}{8\pi^5}\frac{h}{[(X_{s1}+\Re/2)^2+X_{s2}^2]^{1/2}}\left(\frac{h\delta_*}{a^2}\right)\left(\frac{v_*}{U}\right)^4\frac{(\omega\delta_*/U_j)^2|\mathscr{I}_{\pm}(\omega/U_{jc})|^2}{[(\omega\delta_*/U_j)^2+\alpha_p^2]^{3/2}}, \tag{40}$$

where $\delta_*$ and $v_*$ are the boundary layer displacement thickness and friction velocity in the Coanda jet flow from the slot.

The values of $|\mathscr{I}_{\pm}(\omega/U_{jc})|^2$ must be found by numerical integration, as before. However, the following special cases may be noted:

$$|\mathscr{I}_+(k)|^2 = \begin{cases} 3\Gamma^2\left(\frac{5}{3}\right)\Big/\left[\frac{2|k|h\sqrt{1/\mu-1}}{3\pi\mu}\right]^{4/3}, & |k|\Delta\gg 1, \quad \Delta\neq 0; \\ 2\pi^2/[|k|h(1-\mathrm{e}^{-2|k|h})], & \Delta = 0; \end{cases} \tag{41}$$

$$|\mathscr{I}_-(k)|^2 = \begin{cases} 3\Gamma^2\left(\frac{5}{3}\right)\mathrm{e}^{-2|k|h}\Big/\left[\frac{2|k|h\sqrt{1/\mu-1}}{3\pi\mu}\right]^{4/3}, & |k|\Delta\gg 1, \quad \Delta\neq 0; \\ 2\pi^2\mathrm{e}^{-2|k|h}/[|k|h(1-\mathrm{e}^{-2|k|h})], & \Delta = 0. \end{cases} \tag{42}$$

## 5. NUMERICAL RESULTS

To illustrate the predictions of these formulae we consider a typical application involving a nominally elliptic hydrofoil at zero mean angle of attack with semi-major and minor axes $a = 1{\cdot}5$ m and $b = 0{\cdot}2a$, respectively, and with a rounded trailing edge of radius $\Re$. The following parameter values are representative of what might be encountered when a Coanda jet is used to generate a lift coefficient $C_L \sim 3{\cdot}5$ in water at a forward speed of $U = 5$ knots (2·5 m/s):

$$h = 0{\cdot}006a, \quad \Re = 0{\cdot}08a, \quad \{(X_{s1}+\Re/2)^2+X_{s2}^2\}^{1/2} = 0{\cdot}1a, \quad U_o = 2{\cdot}8U,$$

$$U_j = 6U, \quad U_s = 0{\cdot}4U_j. \tag{43}$$

It is assumed that entrainment by the jet produces a local increase in the exterior mean velocity $U_s$ near the slot; the choice $U_s = 0{\cdot}4U_j$ is based on the experimental data of Novak *et al.* [8–10]. For the exterior boundary layer flow we can estimate that near the slot and the rounded trailing edge the displacement thickness $\delta_* \approx 0{\cdot}004a$. Under ideal conditions the Coanda jet is laminar just upstream of the slot exit; we call this case (a), in which there is no direct contribution to the sound from the interaction of the jet with the slot lip. However, according to the observations of Novak *et al.* [8–10] turbulence velocities of magnitude $\sim 0{\cdot}1U_j$ occur near the slot exit, where the same data indicates that the boundary layer

thickness $\sim 0{\cdot}15h$; we call this case (b) and take $\delta_* \approx 0{\cdot}15h/8 = 0{\cdot}019h$ [27]. The friction velocity is taken to be related to the local mean stream velocity $V$ just outside the corresponding turbulent boundary layer by $v_* = 0{\cdot}035V$ (we take $V = U_j$ in the Coanda jet) [27]. It should be noted, however, that this assumption may represent an underestimate, in that significant increases may occur in the turbulence wall shear stress as a result of mean streamline curvature. Thus, the following estimates may need to be revised (by appropriately modifying the magnitude of $v_*$ in equations (20), (33) and (40)) in the light of more accurate turbulence data.

Equations (20), (33) and (40) may now be used to calculate the acoustic pressure frequency spectrum for cases (a) and (b) for prescribed values of the lip thickness $\Delta$. The solid curves in Figures 5 and 6 represent predictions of the overall sound pressure spectrum,

$$10 \times \log_{10}\left(\frac{(U/a)\Phi(\mathbf{x}, \omega)}{(\rho_0 U^2)^2 (La/|\mathbf{x}|^2) M \sin^2(\theta/2) \sin\psi}\right) \text{dB},$$

in these two cases for a lip of zero thickness ($\Delta = 0$) where, respectively for cases (a) and (b), $\Phi(\mathbf{x}, \omega) = \Phi_0(\mathbf{x}, \omega) + \Phi_S(\mathbf{x}, \omega)$ and $\Phi(\mathbf{x}, \omega) = \Phi_0(\mathbf{x}, \omega) + \Phi_S(\mathbf{x}, \omega) + \Phi_J^-(\mathbf{x}, \omega) + \Phi_J^+(\mathbf{x}, \omega)$. The broken line curves in the figure represent the individual contributions from the curvature noise $\Phi_0$, the passive slot noise $\Phi_S$ and (in Figure 6) the Coanda jet–slot interaction $\Phi_J^{\pm}$. The very low-frequency sound is dominated by the curvature noise. At high frequencies the passive slot noise is dominant in case (a), but Figure 6 shows that when turbulence is present in the Coanda jet the spectrum is extended out to much higher frequencies attributable to the interaction of the jet turbulence with the lip. In case (b), and for these particular parameter values, the relative contribution from the passive slot noise is

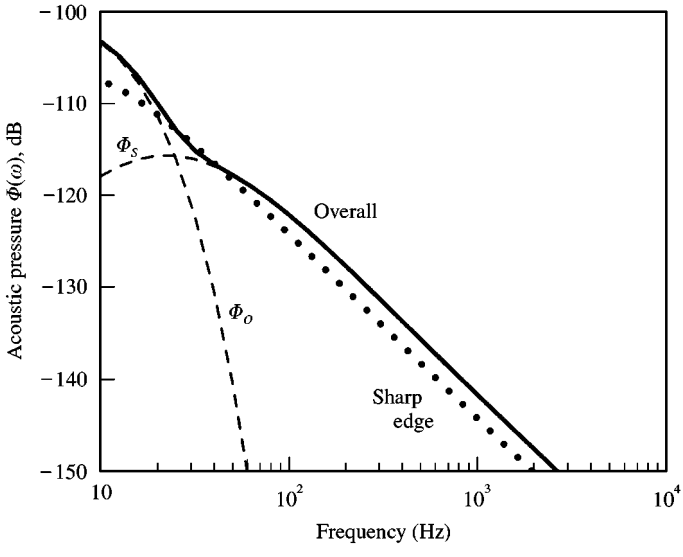


Figure 5. Overall acoustic pressure frequency spectrum (——),

$$10 \times \log_{10}\left(\frac{(U/a)\Phi(\mathbf{x}, \omega)}{(\rho_0 U^2)^2 (La/|\mathbf{x}|^2) M \sin^2(\theta/2) \sin\psi}\right)$$

and the component spectra $\Phi_0$, $\Phi_S$ (– – – –) for conditions (43) for a turbulence-free Coanda jet (Case (a)) and a lip of thickness $\Delta = 0$. The dotted curve (●●●) is the corresponding edge noise spectrum (44) for a flat-plate hydrofoil of equal chord.

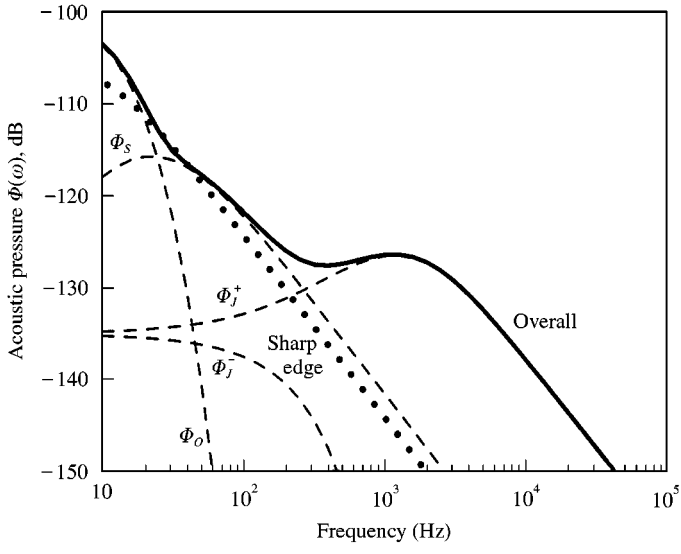


Figure 6. Overall acoustic pressure frequency spectrum (——),

$$10\times\log_{10}\left(\frac{(U/a)\Phi(\mathbf{x},\omega)}{(\rho_0U^2)^2(La/|\mathbf{x}|^2)M\sin^2(\theta/2)\sin\psi}\right)$$

and the component spectra $\Phi_O$, $\Phi_S$, $\Phi_J^{\pm}$ (– – – –) for conditions (43) for a turbulent Coanda jet (Case (b)) and a lip of thickness $\Delta = 0$. The dotted curve (●●●) is the corresponding edge noise spectrum (44) for a flat-plate hydrofoil of equal chord.

negligible. In both cases, $\Phi(\mathbf{x},\omega)$ is predicted to decrease with $f=\omega/2\pi$ like $\Phi_{pp}(\omega)/\omega\sim f^{-2}$ at high frequencies.

At frequencies below about 500 Hz the assumption used in the calculation that the acoustic wavelength is large compared to the hydrofoil chord ceases to be valid, and results at these frequencies should strictly be corrected by application of the interpolation factor given in reference [24]. The correction would decrease the amplitude of the sound predicted at lower frequencies, because of the reduced efficiency with which sound is produced by a hydrofoil of compact chord. The magnitude of the low-frequency correction depends strongly on the radiation direction but, because the fluid–surface interaction mechanism is independent of the chord for small-scale turbulence, we can obtain an overall picture of the importance of trailing edge rounding and the slot-generated sound at these frequencies by comparing our present predictions for a *non-compact* chord with the corresponding predictions for a flat-plate hydrofoil of the same chord, with the same turbulent flow over its trailing edge. For such a flat-plate hydrofoil the mean flow velocity outside the boundary layer is constant and equal to $U$, and for turbulent flow on one side only, we find [17]

$$\frac{(U/a)\Phi(\mathbf{x},\omega)}{(\rho_0U^2)^2(La/|\mathbf{x}|^2)M\sin^2(\theta/2)\sin\psi}\approx\frac{0{\cdot}7}{2\pi^2}\left(\frac{\delta_*}{a}\right)^2\left(\frac{v_*}{U}\right)^4\frac{(\omega\delta_*/U)}{[(\omega\delta_*/U)^2+\alpha_p^2]^{3/2}}.\qquad(44)$$

This is plotted as the dotted curves in Figures 5 and 6. Comparison with the spectrum for the overall CC-hydrofoil noise reveals a broad level of agreement at very low frequencies, and also at high frequencies when the Coanda jet is turbulent-free. However, at high frequencies the radiation generated by the turbulent Coanda jet is typically 20 dB in excess of the flat-plate edge noise.

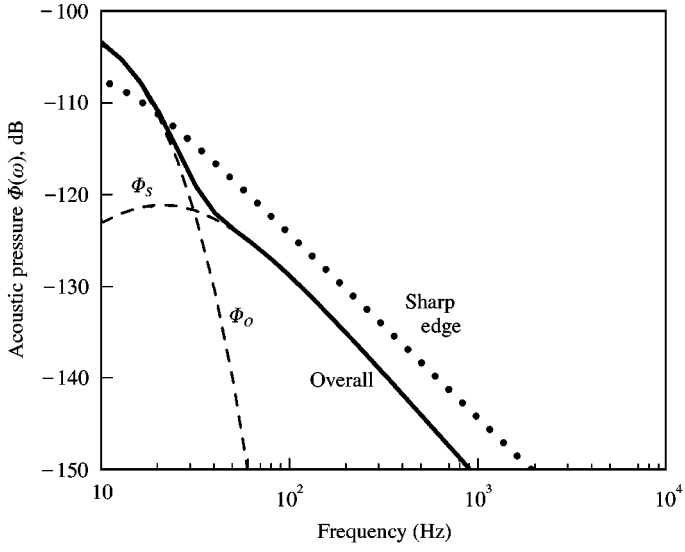


Figure 7. Overall acoustic pressure frequency spectrum (——),

$$10 \times \log_{10}\left(\frac{(U/a)\Phi(\mathbf{x}, \omega)}{(\rho_0 U^2)^2 (La/|\mathbf{x}|^2) M \sin^2(\theta/2) \sin\psi}\right)$$

and the component spectra $\Phi_O$, $\Phi_S$ (– – – –) for conditions (43) for a turbulence-free Coanda jet (Case (a)) and a lip of thickness $\Delta = 0{\cdot}5h$. The dotted curve (●●●) is the corresponding edge noise spectrum (44) for a flat-plate hydrofoil of equal chord.

Figures 7 and 8 display the corresponding predictions, respectively, for cases (a) and (b) when the slot lip has thickness $\Delta = 0{\cdot}5h$. In case (a) (no jet turbulence), the passive slot noise is smaller (relative to the case $\Delta = 0$) by about 5 dB at low frequencies; the reduction is larger at high frequencies because the finite thickness of the lip causes the spectrum to decrease like $\Phi_{pp}(\omega)/\omega^{4/3} \sim f^{-7/3}$ (instead of like $f^{-2}$ when $\Delta = 0$); the efficiency of production of sound at the slot is in this case smaller than for the corresponding flat-plate edge flow represented by the dotted curve. When the Coanda jet is turbulent (Figure 8, Case(b)) the higher frequencies are once again dominated by the jet–slot interaction noise (which also decreases like $f^{-7/3}$).

## 6. CONCLUSION

Coanda wall jet circulation control permits the lift generated by a hydrofoil to be greatly increased at low mean flow speeds without the deployment of mechanical lift augmentation devices such as a trailing edge flap. However, because of the relatively high jet speeds required to maintain attached flow around the hydrofoil, additional self-noise is produced over and above that usually attributed to the boundary layer turbulence (generated by boundary layer instability even when the incident mean flow is nominally steady) interacting with the trailing edge.

Three noise sources that are likely to dominate the production of sound in vicinity of the trailing edge of the hydrofoil have been identified. Theoretical predictions of their relative contributions to the overall self-noise of the CC-hydrofoil are critically dependent on a proper understanding of the turbulence characteristics of the flow, especially within the

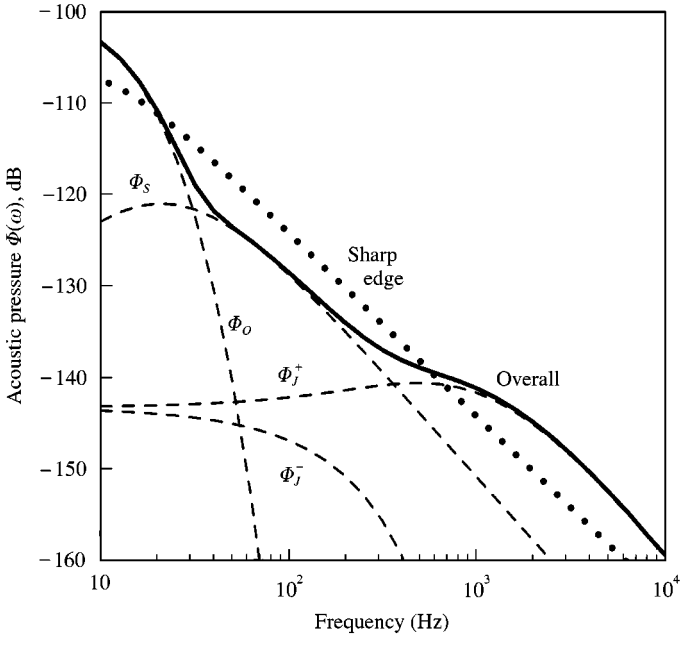


Figure 8. Overall acoustic pressure frequency spectrum (——),

$$10 \times \log_{10}\left(\frac{(U/a)\Phi(\mathbf{x}, \omega)}{(\rho_0 U^2)^2 (La/|\mathbf{x}|^2) M \sin^2(\theta/2) \sin\psi}\right)$$

and the component spectra $\Phi_o$, $\Phi_S$, $\Phi_J^{\pm}$ (– – – –) for conditions (43) for a turbulent Coanda jet (Case (b)) and a lip of thickness $\Delta = 0{\cdot}5h$. The dotted curve (●●●) is the corresponding edge noise spectrum (44) for a flat-plate hydrofoil of equal chord.

Coanda jet. The following quantitative conclusions are based on particular numerical estimates for these quantities used in this paper, and should therefore be regarded as tentative.

Very low frequencies are dominated by "curvature noise", generated by the interaction of boundary layer turbulence with the rounded trailing edge of the CC-hydrofoil; it is similar in character and amplitude to the low-frequency component of the trailing edge noise produced by a hydrofoil of equal chord, but with a sharp trailing edge. The jet slot is the main source at higher frequencies. "Passive slot noise" is produced by the "scattering" into sound of the nearfield pressure fluctuations of turbulence in the exterior mean boundary layer flow over the slot. This is much stronger than the curvature noise at higher frequencies, and is comparable in magnitude to the sharp edged trailing edge noise. However, if the Coanda jet is turbulent, the sound produced by its interaction with the lip of the slot tends to be the dominant source at high frequencies (say for $fh/U_j > 1$). The overall level of the interaction noise depends on the thickness $\Delta$ of the slot lip: when $\Delta = 0$ the Coanda jet noise at higher frequencies is typically 20 dB or more greater than conventional trailing edge noise. The difference becomes smaller as the lip increases in thickness, since this tends to reduce the efficiency of the edge scattering.

It has been implicitly assumed that the acoustic impedance of the jet slot is infinitely large. This means that no account is taken of "cavity resonances" of the jet plenum. Such resonances probably occur in practice at very low frequencies. In principle, their

contributions can be included by modifying the hydroacoustic Green function in the manner described in reference [29], although the modification would depend on a detailed specification of the plenum characteristics and would be useful only if observation indicated the presence of resonance peaks in the acoustic spectrum.

## ACKNOWLEDGMENT

The work reported in this paper is supported by the Office of Naval Research under Grant N00014-00-1-0127 administered by Dr L. Patrick Purtell. The author gratefully acknowledges the benefit of discussions with Dr Jane S. Abramson, Dr William K. Blake, Dr Theodore M. Farabee and Dr Ernest O. Rogers.

## REFERENCES

1. H. COANDA 1932 *Brevet Invent. Gr Cl.* 2 *No.* 762688 *République Française*. Procédé de propulsion dans un fluide.
2. P. W. CARPENTER and P. N. GREEN 1997 *Journal of Sound and Vibration* **208**, 777–802. The aeroacoustics and aerodynamics of high-speed Coanda devices. Part I: conventional arrangement of exit nozzle and surface.
3. L. J. PRITCHARD 1957 *Journal of the Royal Aeronautical Society* **61**, 149–180. The dawn of aerodynamics.
4. R. WILLE and H. FERNHOLZ 1965 *Journal of Fluid Mechanics* **23**, 801–819. Report on the first European Mechanics Colloquium on the Coanda effect.
5. R. J. ENGLAR and C. A. APPLEGATE 1984 *David Taylor Naval Ship Research and Development Center Report No. DTNSRDC* 84/052, *Bethesda, MD*. Circulation control—a bibliography of DTNSRDC research and selected outside references (Jan 1969–Dec. 1983).
6. I. C. CHEESEMAN and A. R. SEED 1996 *Journal of the Royal Aeronautical Society* **71**, 451–467. The application of circulation control by blowing to helicopter rotors.
7. N. J. WOOD and J. N. NIELSEN 1986 *American Institute of Aeronautics and Astronautics Journal* **23**, 865–875. Circulation control airfoils as applied to rotary-wing aircraft.
8. C. J. NOVAK and K. C. CORNELIUS 1986 *Lockheed-Georgia Company Report L87R0618* Vol. II: Advanced (circulation control) airfoil performance and analysis: experimental program summary.
9. C. J. NOVAK and K. C. CORNELIUS 1986 *Lockheed-Georgia Company Report L87R0618* Vol. III: Advanced (circulation control) airfoil performance and analysis: experimental program data.
10. C. J. NOVAK, K. C. CORNELIUS and R. K. ROADS 1987 *American Institute of Aeronautics and Astronautics Paper* 87-0155. Experimental investigation of the circular wall jet on a circulation control airfoil.
11. J. N. NIELSEN (editor) 1987 *Proceedings of the Circulation Control Workshop* 1986, NASA Conference Publication 2432.
12. A. ZANDIEH and J. G. LEISHMAN 1993 *American Institute of Aeronautics and Astronautics Journal* **31**, 1769–1776. Boundary layer and pressure measurements on a circular cylinder with unsteady circulation control.
13. V. RAGHAVAN, I. CHOPRA and S. PAI 1988 *Journal of the American Helicopter Society* **33**, 28–37. Circulation control airfoils in an unsteady flow.
14. M. SALIKUDDEN, W. H. BROWN and K. K. AHUJA 1987 *Journal of Aircraft* **24**, 55–64. Noise from a circulation control wing with upper surface blowing.
15. P. W. CARPENTER and C. SMITH 1997 *Journal of Sound and Vibration* **208**, 803–822. The aeroacoustics and aerodynamics of high-speed Coanda devices. Part II: effects of modifications for flow control and noise reduction.
16. M. J. LIGHTHILL 1952 *Proceedings of the Royal Society* **A211**, 564–587. On sound generated aerodynamically. Part I: general theory.
17. M. S. HOWE 1998 *Acoustics of Fluid–Structure Interactions*. Cambridge: Cambridge University Press.
18. M. S. HOWE 1999 *Journal of Sound and Vibration* **225**, 211–238. Trailing edge noise at low Mach numbers.

19. G. K. BATCHELOR 1967 *An Introduction to Fluid Dynamics*. Cambridge: Cambridge University Press.
20. D. M. CHASE 1972 *Journal of the Acoustical Society of America* **52**, 1011–1023. Sound radiated by turbulent flow off a rigid half-plane as obtained from a wavevector spectrum of hydrodynamic pressure.
21. D. M. CHASE 1975 *American Institute of Aeronautics and Astronautics Journal* **13**, 1041–1047. Noise radiated from an edge in turbulent flow.
22. K. L. CHANDIRAMANI 1974 *Journal of the Acoustical Society of America* **55**, 19–29. Diffraction of evanescent waves, with applications to aerodynamically scattered sound and radiation from unbaffled plates.
23. W. R. SEARS 1941 *Journal of the Aeronautical Sciences* **8**, 104–108. Some aspects of non-stationary airfoil theory and its practical applications.
24. M. S. HOWE 2001 *Quarterly Journal of Mechanics and Applied Mathematics* **54**, 139–155. Edge-source acoustic Green's function for an airfoil of arbitrary chord, with application to trailing edge noise.
25. D. M. CHASE 1980 *Journal of Sound and Vibration* **70**, 29–67. Modeling the wavevector-frequency spectrum of turbulent boundary layer wall pressure.
26. G. M. CORCOS 1964 *Journal of Fluid Mechanics* **18**, 353–378. The structure of the turbulent pressure field in boundary layer flows.
27. J. O. HINZE 1975 *Turbulence*. New York: McGraw-Hill; second edition.
28. H. LAMB 1932 *Hydrodynamics* (Reprinted 1993). Cambridge: Cambridge University Press; sixth edition.
29. M. S. HOWE 1976 *Journal of Sound and Vibration* **45**, 427–440. On the Helmholtz resonator.